Quaternary Science Reviews 223 (2019) 105945

Contents lists available at ScienceDirect

Quaternary Science Reviews

journal homepage: www.elsevier.com/locate/quascirev

Evolution of Antarctic Intermediate Water during the Plio-Pleistocene and implications for global climate: Evidence from the South Atlantic

Cyrus Karas [a, b, c, *], Steven L. Goldstein [a, d], Peter B. deMenocal [a, d]

[a] Lamont Doherty Earth Observatory of Columbia University, Palisades, NY 10964, USA
[b] Instituto de Geografía, Pontificia Universidad Católica de Chile, Santiago, Chile
[c] Millennium Nucleus Paleoclimate, University of Chile, Santiago, Chile
[d] Department of Earth and Environmental Sciences, Columbia University, Palisades, NY 10964, USA

ARTICLE INFO

Article history:
Received 14 May 2019
Received in revised form
13 September 2019
Accepted 14 September 2019
Available online xxx

ABSTRACT

Formed in the Southern Ocean, Antarctic Intermediate Water (AAIW) plays a fundamental role in the modern climate system as an important sink for atmospheric CO_2, and as a mid-depth conduit supplying nutrient-rich waters to subtropical and tropical upwelling regions. During the transition from warm Pliocene 'greenhouse' conditions to Pleistocene 'icehouse' conditions around 3 Ma, model simulations suggest dramatic circulation changes in the Southern Ocean AAIW formation region due to cooling and expanded sea ice cover around Antarctica. However, the history and properties of AAIW over this time period are still poorly understood. Here, we trace AAIW source water provenance, temperature, and salinity changes over the last 4 Myr using Nd isotopes of Fe-Mn-oxyhydroxide encrusted foraminifera, benthic foraminiferal Mg/Ca, and stable isotopes from southwest Atlantic DSDP Site 516. Our results show that modern AAIW properties emerged gradually over the last 3 Myr, as evidenced by gradual cooling (6 °C) and freshening of intermediate waters. Over this same interval, εNd-values decrease and diverge away from those of Pacific-sourced waters and converge on values of present-day Circumpolar Deep Water (CDW). These observations are in accordance with model simulations indicating increased deep vertical mixing at the Polar Front associated with sea ice extension. These modified AAIW source waters penetrated increasingly northward into the Atlantic at intermediate depths, enhancing nutrient supply and contributing to surface cooling along subtropical coastal upwelling sites. These circulation changes may have facilitated ocean CO_2 storage, providing a positive feedback amplifying global cooling and intensification of Northern Hemisphere Glaciation.

1. Introduction

Antarctic Intermediate Water (AAIW) is a cool (~2–5 °C) and low-salinity (~34.4 psμ) water mass that originates from an area between 45 and 55°S, extending from the Antarctic Polar Front towards the north of the Subantarctic Front (McCartney, 1977; Talley, 1996). There it is formed by vertical mixing with upwelled Circumpolar Deep Water (CDW) during the Austral winter, and after subduction its core flows northward at intermediate (700–1200 m) water depths in all three ocean basins (McCartney, 1977; Piola and Georgi, 1982; Tsuchiya, 1989; Talley, 1996; Sarmiento et al., 2004; Pellichero et al., 2018 and refs. therein). Hence, AAIW is an important part of the thermohaline ocean circulation and represents the shallow arm of the cold water route from the Southern to the Northern Hemisphere for balancing the southward flow of North Atlantic Deep Water (NADW) from the North Atlantic Ocean (e.g., Talley, 2013).

Two interlinked main processes have been proposed to drive the formation, and northward drift of AAIW. One is the well-known wind-driven upwelling and Ekman transport occurring during the present-day, and the last glacial and interglacial (Wainer et al., 2012 and refs therein). The other is seasonal sea ice formation and melting close to Antarctica that drive buoyancy changes in the Southern Ocean (Abernathey et al., 2016; Evans et al., 2018; Pellichero et al., 2018). In the Southwest Atlantic Ocean, AAIW is mainly derived from the Southeast Pacific Ocean, flowing through the Drake Passage and then northward towards the area of DSDP Site 516 (McCartney, 1977; Piola and Matano, 2001, Fig. 1a; location:

* Corresponding author. Lamont Doherty Earth Observatory of Columbia University, Palisades, NY 10964, USA.
E-mail address: cyrus.karas@uc.cl (C. Karas).

https://doi.org/10.1016/j.quascirev.2019.105945
0277-3791/

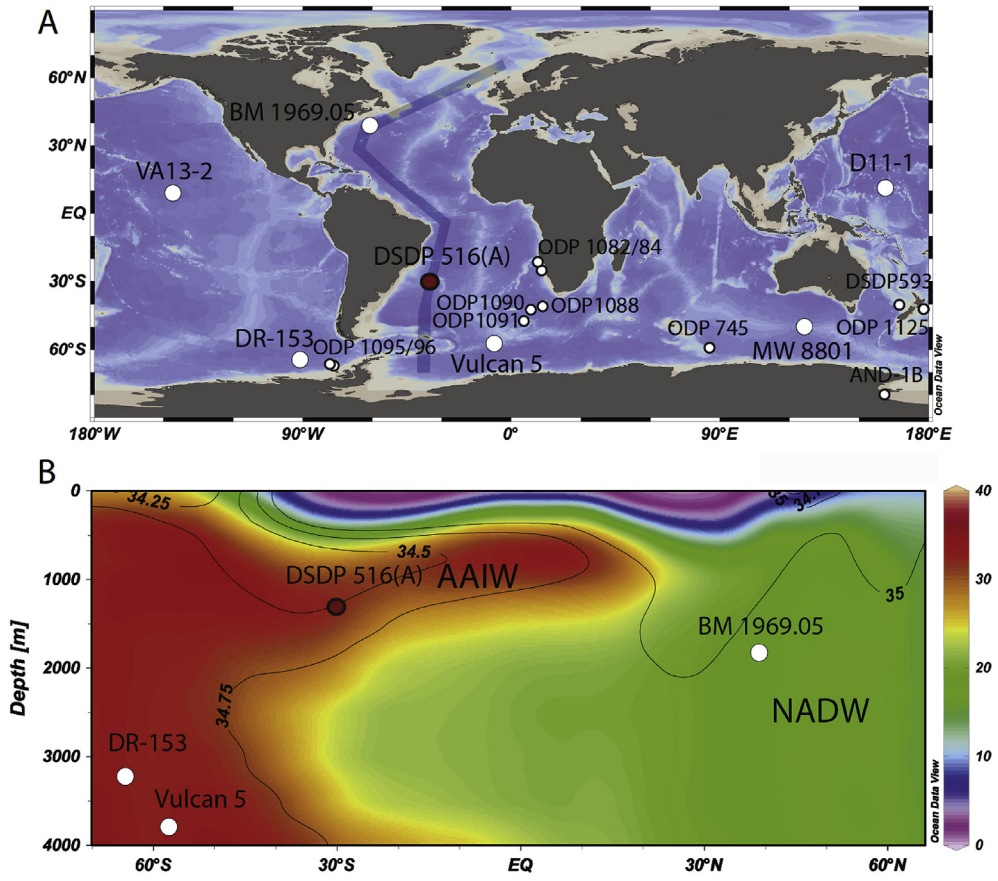

Fig. 1. Location of core sites and water masses in the Atlantic. a) Map showing locations of Site 516 and other sites in the text. The shaded line indicates the Atlantic depth profile shown in b), showing nutrient contents (nitrate in μmol/mol) in color shading and salinity (in psu) in contour lines (Antonov et al., 2010; Garcia et al., 2010). AAIW, NADW and core sites are indicated. Figure is made with Ocean Data View (Schlitzer, 2012; version 4.51; http://odv.awi.de). (For interpretation of the references to color in this figure legend, the reader is referred to the Web version of this article.)

30°17′S; 35°17′W; 1313 m water depth).

Large amounts of anthropogenic CO_2 are stored in Southern Ocean surface and subsurface waters through AAIW formation as well as its subsurface flow domains in the Atlantic, Pacific, and Indian Ocean sectors (Sabine et al., 2004). Even though there is upwelling of CDW close to Antarctica that releases CO_2 into the atmosphere (not fully sequestered by bio-productivity) there is still a net transport of atmospheric CO_2 into the Southern Ocean (Gruber et al., 2009). Hence, during past times of positive ocean-atmosphere CO_2 disequilibria, AAIW formation can be expected to have been an important water mass for facilitating carbon uptake and sequestration on short time scales.

AAIW is also a nutrient rich water mass that ventilates the thermocline of upwelling regions, together with shallower sub-antarctic mode waters, in the tropics and subtropics (Toggweiler et al., 1991; Gordon et al., 1992). The high nutrient content of these waters fuel biological productivity in these regions where the biologic pump can sequester carbon through sedimentary carbon burial, a process active both today and in the geologic past (Sarmiento et al., 2004; Cortese et al., 2004; Etourneau et al., 2012; Winckler et al., 2016).

During the 'Plio-Pleistocene climate transition', which is the gradual climatic change from Pliocene greenhouse conditions towards the onset of Northern Hemisphere Glaciation, resulting in larger and bipolar glacial cycles since around 3 Ma, several studies have proposed that there is a linkage to increased subsurface delivery of cooler, nutrient-rich waters from the Southern Ocean via AAIW to lower-latitude upwelling sites (Marlow et al., 2000; Lawrence et al., 2006; Etourneau et al., 2009, 2012). These nutrients would have fuelled primary productivity of diatoms and resulting in enhanced CO_2 uptake in these regions during this Plio-Pleistocene cooling period between 3 and 2 Ma (Etourneau et al., 2012). Moreover, by ~1.8 Ma, distinct cooling of AAIW source regions has been linked to a coeval cooling of the equatorial East Pacific Ocean, indicating that AAIW may have directly cooled this region by upwelling as a result of increased wind speeds (Martinez-Garcia et al., 2010).

At the same time it has been suggested that the Southern Ocean upwelling of CDW and AAIW formation considerably strengthened (McKay et al., 2012; Hill et al., 2017). There is evidence for polar sea surface cooling close to Antarctica and sea ice extension in the Ross Sea around 3.3 Ma, as recorded by sediment core AND-1B in the Ross Sea and other opal records (a proxy for ocean stratification) from the Atlantic sector of the Southern Ocean such as ODP Site 1096 (McKay et al., 2012; Hillenbrand and Cortese, 2006; locations in Fig. 1). Cooling of mid-polar latitudes compared to the tropics caused an increase in the meridional temperature gradient, resulting in increased zonal westerly wind speeds (Brierley et al., 2009; Fedorov et al., 2013), which in turn was likely important for AAIW formation and subduction (Wainer et al., 2012 and refs therein). In fact, climate model simulations (Hill et al., 2017) show that expanded Ross Sea sea ice extent invigorated and broadened austral westerly wind circulation. The stronger westerlies promoted vertical mixing of water masses in the Southern Ocean and

enhanced upwelling of CDW (Hill et al., 2017). The same relationship, that is, between increased westerly wind speeds and increased circulation in the Southern Ocean, has been suggested by an eddy-resolving simulation for the present-day (Bishop et al., 2016).

Despite these climate simulation studies and proposed changes in AAIW provenance and properties across the Plio-Pleistocene climate transition, there are until now no proxy records of late Neogene changes in AAIW in the Atlantic Ocean. To elucidate both the development of AAIW in the South Atlantic Ocean and the telecommunication of AAIW with subtropical upwelling regions, we here present the first proxy records of Atlantic AAIW over the last four million years. Using sediments from South Atlantic DSDP Site 516, we present a multiproxy approach that tracks water mass provenance using neodymium (Nd) isotope ratios in Fe-Mn encrusted foraminifera, bottom water temperatures (BWT) from benthic foraminiferal (*Uvigernina peregrina* and *Cibicidoides wuellerstorfi*) Mg/Ca, and salinity derived from benthic oxygen isotopes and the Mg/Ca-derived BWT.

2. Materials and methods

2.1. Benthic stable isotope and Mg/Ca analysis of Site 516 and 516 (A)

For preparation of samples for $\delta^{18}O$ and Mg/Ca analyses we followed previous studies (Karas et al., 2009, 2017). Our Site 516 samples span the time period over the last 4 Myr. We used the >250 μm size fraction. Each sample represents 4–34 specimens of *Uvigerina peregrina*. The samples were gently crushed and visually separated under a microscope. Approximately two-thirds of each initial sample was used for Mg/Ca analyses with one-third reserved for stable isotope analyses. One to three specimens of *Cibicidoides wuellerstorfi* from Site 516 were used for stable isotope analyses. Stable isotope analyses ($\delta^{18}O$) at Site 516 were conducted at Lamont-Doherty Earth Observatory (LDEO) on a Thermo Delta V Plus stable isotopic ratio mass spectrometer with a Thermo Kiel IV carbonate device. The long-term analytical precision for $\delta^{18}O$ is ±0.06. All $\delta^{18}O$ values of *C. wuellerstorfi* were corrected by +0.64‰ (Duplessy et al., 1984).

Site 516A samples span the time period of ~2.8–4 Myr. We performed Mg/Ca analyses using 9–32 specimens from *U. peregrina* or *C. wuellerstorfi*. All cleaning before Mg/Ca analyses included a reductive step (Barker et al., 2003). Elemental analyses of foraminiferal specimens were carried out at LDEO on a ThermoFisher iCapQ 6500 quadrupole ICPMS. Long-term Mg/Ca analytical reproducibility for an internal standard was ±0.09 mmol/mol (3.6%) with an accuracy of 0.8%.

Following previous down-core studies from the Plio-Pleistocene in the Southern Hemisphere (McClymont et al., 2016; Elmore et al., 2015) we used a species-specific temperature calibration (Elderfield et al., 2006), $Mg/Ca = 0.9\ exp\ (0.11T)$, to transfer Mg/Ca values of *C. wuellerstorfi* into BWT. For the calculation of Mg/Ca values of *U. peregrina* into BWT we used a species-specific calibration (Elderfield et al., 2010), $Mg/Ca = 1 + 0.1\ T$ (0.1 mmol/°C). Accounting for our analytical error of 0.09 mmol/mol, we estimate a total propagated error of approximately ±1 °C. The preservation of foraminiferal tests at Site 516A has been discussed previously and was suggested to be very good, with negligible dissolution effects on foraminiferal Mg (Karas et al., 2017). The effect of temporal changes in Mg/Ca of seawater on the Mg/Ca of specific benthic species is still unclear and different species might have different Mg/Ca seawater - Mg/Ca test relationships (Evans et al., 2016). Estimations of differences in Mg/Ca derived BWT reconstructions for the Pliocene indicate they are small, ranging from no significant changes for the BWT of *U. peregrina* to an underestimation of ~1 °C for BWT of other species (Evans et al., 2016). Hence, we do not further correct our initial benthic Mg/Ca ratios but note that our Pliocene benthic temperatures might be slightly underestimated.

2.2. Nd isotope analyses

For εNd analyses we selected approximately 25–40 mg of mixed foraminiferal species (>1000 specimens) from the 250–315 μm size fraction. Samples were crushed between two glass plates under a microscope. In order to avoid measuring non-authigenic Nd carried by detrital phases detrital phases (e.g., Wilson et al., 2013; Elmore et al., 2011), prior to dissolution all samples were ultrasonically cleaned and rinsed with methanol and MilliQ® water until they were visibly free of detrital material, while Fe-Mn oxides were not removed. After dissolution in 1N HNO_3 and ultrasonication, samples were centrifuged for 2–3 min and Nd was separated using Eichrom Tru-Spec and Ln-Spec resins. Neodymium isotope ratios were measured on a ThermoScientific Neptune-Plus® multiple collector inductively coupled plasma mass spectrometer (MC-ICPMS) at LDEO. Instrumental mass bias was corrected using $^{146}Nd/^{144}Nd = 0.7129$ using an exponential mass fractionation law. All sample measurements were bracketed by measurements of the JNdi standard (20 ppb) to monitor instrumental drift, and corrected to a value of $^{143}Nd/^{144}Nd = 0.512115$ for JNdi (Tanaka et al., 2000). The mean error of 28 JNdi standards is ±0.000013 (26 ppm; 2σ-standard deviation), equivalent to ± 0.26 εNd-units (2σ). External reproducibility is expressed as a combined error of the JNdi error and an internal error and is ±0.38 (2σ) for 21 samples (see Table S1). Nd isotope ratios are reported as $^{143}Nd/^{144}Nd$ and as εNd, the deviation of the $^{143}Nd/^{144}Nd$ ratio of the sample in parts per 10^4 from 0.512638, an estimate of the average value of chondrites (Jacobsen and Wasserburg, 1980) ((i.e. $[(^{143}Nd/^{144}Nd_{sample}/0.512638) - 1) * 10^4]$). Data are listed in Supplementary Materials (Table S1).

2.3. Establishing an age model for Site 516

For establishing a robust age model for Site 516 we followed the procedure of earlier studies using the mbsf (meters below sea floor) scale, as spliced records do not exist for DSDP core sites (Karas et al., 2009, 2017). Accordingly, due to several potential coring problems in the beginning of each core segment we omitted mbsf depths when they overlapped (Karas et al., 2017). Sediment recovery was 84–100% in the sampled cores (Barker et al., 1983).

In a first step, selected depths of foraminiferal and calcareous nannofossil datums were obtained over the last 5 Myr (Barash et al., 1983; Berggren et al., 1983) and ages were updated to the astronomically tuned Neogene time scale (ATNTS; Lourens et al., 2004) (the age-depth plot is given in Fig. 2a). For establishing an initial age-depth relationship we gave preference (if available) to the nannofossil biodatums.

To refine the initial age model during the time period 3.86–0 Myr we produced a mixed benthic $\delta^{18}O$ record of *C. wuellerstorfi* and *U. peregrina*. In the cases of having data from both species in a sample we calculated an average value. The resulting benthic isotope record was matched to global LR04 stack (Lisiecki and Raymo, 2005) with Analyseries2 (Paillard et al., 1996) (Fig. 2b). The correlation coefficient between both is ~0.7.

2.4. Error estimation of the age model

Between 3.86 and 0 Ma our refined age-depth relationship falls within available biostratigraphic control (Barash et al., 1983; Berggren et al., 1983) indicating that the initial biostratigraphy only needed small adjustments using the benthic isotope stratigraphy

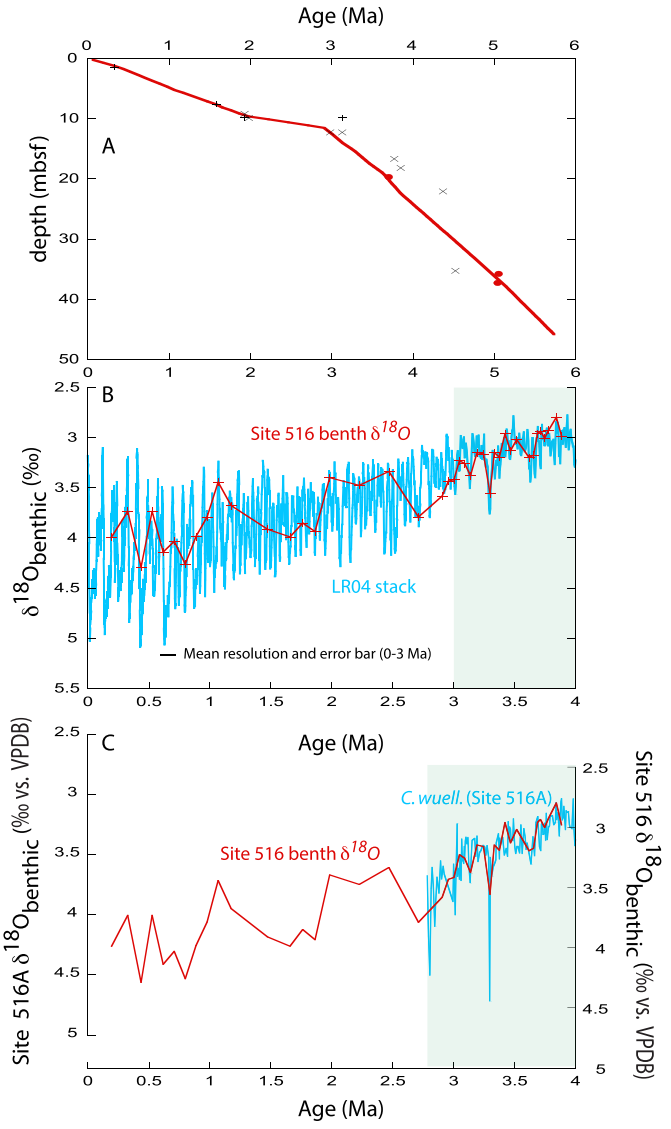

Fig. 2. Age model of Site 516. a) Foraminiferal biodatums for the time period 3-0 Ma (black crosses; Barash et al., 1983), for the time period 5-2 Ma (black x, Berggren et al., 1983) and nannofossil biodatums (Berggren et al., 1983) (red dots). The final age-depth relationship after tuning our benthic isotope record from Site 516 to the global benthic LR04 stack (Lisiecki and Raymo, 2005) between 0 and 3.86 Ma (red line). b) Benthic isotope record from Site 516 (mixed *C. wuellerstorfi* and *U. peregrina* record; red) after tuning to the global benthic LR04 stack (Lisiecki and Raymo, 2005; blue). C) Comparison of benthic isotope records from Site 516 (mixed *C. wuellerstorfi* and *U. peregrina;* red) and *C. wuellerstorfi* record from Site 516A (Karas et al., 2017; light blue). Error bars are indicated (see methods). (For interpretation of the references to color in this figure legend, the reader is referred to the Web version of this article.)

(Fig. 2a and b). This supports the general robustness of our age model. Between 3.9 and 3.0 Ma our benthic $\delta^{18}O$ record approaches obliquity-scale age resolution with an average resolution of ~44 kyr (25–102 kyr). The resulting age-depth model during this time is further supported by an existing benthic isotope stratigraphy age model at Site 516A (Karas et al., 2017) which shows good agreement (Fig. 2c). For the last 3 Myr, our benthic $\delta^{18}O$ record has on average a lower resolution of 138 kyr (90–297 kyr; Fig. 2b). This uncertainty however, is reduced as during the last 2 Ma the planktonic foraminiferal biostratigraphic data were obtained every 20–25 cm (Barash et al., 1983), which translates into a resolution of 50–62 kyr. Diachronous foraminiferal datums might increase absolute errors.

Between 4.7 and 4.0 Ma, our age model shows a good linear continuation of the earlier time period (Fig. 2a) and is constrained by available nannofossil biodatums, which also leads to a good solution through the foraminiferal biodatums (sample space of biodatums are 1.5 m; Berggren et al., 1983; equivalent to 117 kyr time resolution).

2.5. Calculation of $\delta^{18}O_{seawater}$ and $\delta^{18}O_{IVC\text{-}seawater}$

The calculation of $\delta^{18}O_{seawater}$ from paired Mg/Ca and $\delta^{18}O$ analyses for the whole record of Site 516 uses a well-known equation: $T = 16.9 - 4.38 \times (\delta^{18}O_{foram} - \delta^{18}O_{seawater}) + 0.1 \times (\delta^{18}O_{foram} - \delta^{18}O_{seawater})^2$ (Fig. 3a,b,c; Shackleton, 1974). For the calculation we used bottom Mg/Ca temperatures from *U. peregrina* (T) and a mixed $\delta^{18}O$ record from *U. peregrina* and *C. wuellerstorfi* (Fig. 3a and b). Benthic foraminiferal $\delta^{18}O$ (PDB scale) were adjusted to the SMOW scale by adding 0.27‰ (Hut, 1987). This correction accounts for different fractionations when dissolving carbonate in acid (PDB scale) vs. equilibrating CO_2 in water (SMOW scale; Hut, 1987). As the global ice volume changed considerably over the last ~4 Ma (e.g.

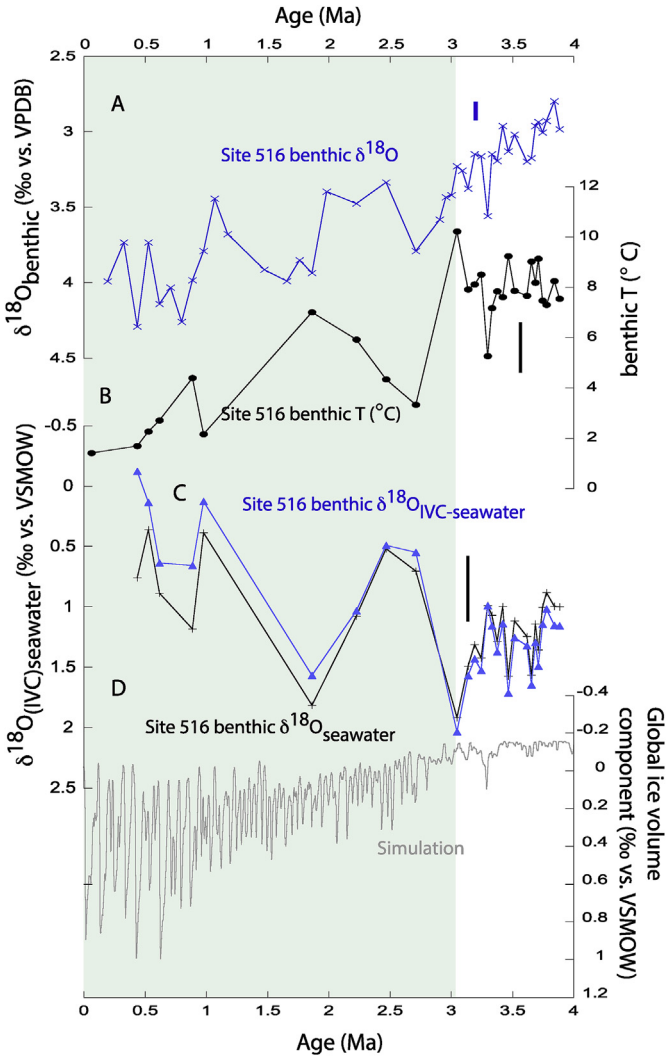

Fig. 3. Calculation of $\delta^{18}O_{seawater}$ and $\delta^{18}O_{IVC\text{-}seawater}$ at Site 516. a) Benthic $\delta^{18}O$ (blue) and b) Mg/Ca temperatures (black) were used to calculate c) $\delta^{18}O_{seawater}$ from Site 516 (black) and ice-volume corrected $\delta^{18}O_{IVC\text{-}seawater}$ (blue). $\delta^{18}O_{IVC\text{-}seawater}$ was obtained by subtracting d) an estimation of the global ice volume change (de Boer et al., 2014). Error bars are indicated (see methods). (For interpretation of the references to color in this figure legend, the reader is referred to the Web version of this article.)

Lisiecki and Raymo, 2005) and we are interested in regional salinity changes, we decided to correct our initial $\delta^{18}O_{seawater}$ over this time for the changes in global ice volume. For an estimation of changes in global ice volume we here used a record based on a model simulation (de Boer et al., 2014, Fig. 3d). This model simulation calculated the ice volume component of the global LR04 stack (relative to present; Lisiecki and Raymo, 2005) by simulating ice sheet extents in the Northern and Southern Hemispheres (de Boer et al., 2014, Fig. 3d). We subtracted this global ice volume estimation from our initial $\delta^{18}O_{seawater}$ record to obtain ice-volume corrected ($\delta^{18}O_{IVC\text{-}seawater}$) values (Fig. 3c and d). The propagated error for calculating $\delta^{18}O_{seawater}$ is about ±0.27‰ (mainly due to a temperature error of ±1 °C). We expect a similar error for our $\delta^{18}O_{IVC\text{-}seawater}$ values, as our global ice volume estimation is based on a model simulation (de Boer et al., 2014).

2.6. Calculation of opal mass accumulation rates (opal MAR) from Site 745

For calculating Opal MAR from Australian-Antarctic Basin Site 745 we updated data from an earlier study (Billups et al., 2013). Opal fluxes were calculated as the product of opal fraction data (from Ehrmann and Grobe, 1991), dry bulk densities (data from Barron and Larsen, 2005), and interval sedimentation rates. For calculating the sedimentation rates we updated an existing age model (Billups et al., 2013). All magnetic reversal age control points were updated to the ATNTS 2004 age scale (Lourens et al., 2004), and in cases of representing short intervals we calculated average values. Finally, the revised age model was created based on simple interpolation between the control points.

3. Results and discussion

3.1. Interpretation of εNd signatures of Site 516

The main source of the Nd in the foraminifera is authigenic Fe-Mn-oxide on the foraminiferal tests. While diagenetic porewaters can influence the εNd signatures on foraminiferal tests, especially in regions with high input of volcanic ashes like in the North Pacific close to Alaska (e.g. Abbott et al., 2015; Du et al., 2016), extracted εNd signatures from foraminifera from many (South) Atlantic sites have been shown to faithfully record ancient bottom water masses in different ocean settings (e.g. Rutberg et al., 2000; Piotrowski et al., 2004, 2005; 2008; Roberts et al., 2010; Kraft et al., 2013) and in the region of Site 516 at the Brazil margin during the last 25 ka (Howe et al., 2016). The Plio-Pleistocene sediments at Site 516 consist of homogeneous light calcareous sandy-oozes (almost entirely foraminifera and coccolithophorides) with only small amounts of clay minerals, and show very low sedimentation rates over the last 3 Ma (0.4 cm/kyr), (Zimmermann, 1983). Regions with such low sedimentation rates, oxic conditions, low organic carbon and carbonate determined environments have been shown to be insensitive to pore water alteration on for earth elements and Nd isotope ratios (Martin and Haley, 2000; Osborne et al., 2017). Moreover, Fe/Ca and Mn/Ca values from non-reductively cleaned planktic foraminifera (an indicator for terrigenous input/diagenesis) show low values of less than 1 mmol/mol for the Pliocene at Site 516A (2.7–5.7 Ma; Karas et al., 2017). The youngest εNd-values at Site 516 of around −7.3 correspond (within errors) to present-day published seawater values from AAIW in the South Atlantic and the Southern Ocean sector of the Atlantic Ocean that show on average εNd of around −8 (Jeandel, 1993; Stichel et al., 2012). Also, Holocene coretop foraminiferal εNd from the Brazil margin from a similar AAIW water depth and location as Site 516 show values around −8 (Howe et al., 2016, Fig. 4a). Hence we interpret the εNd as reflecting ancient bottom water signals.

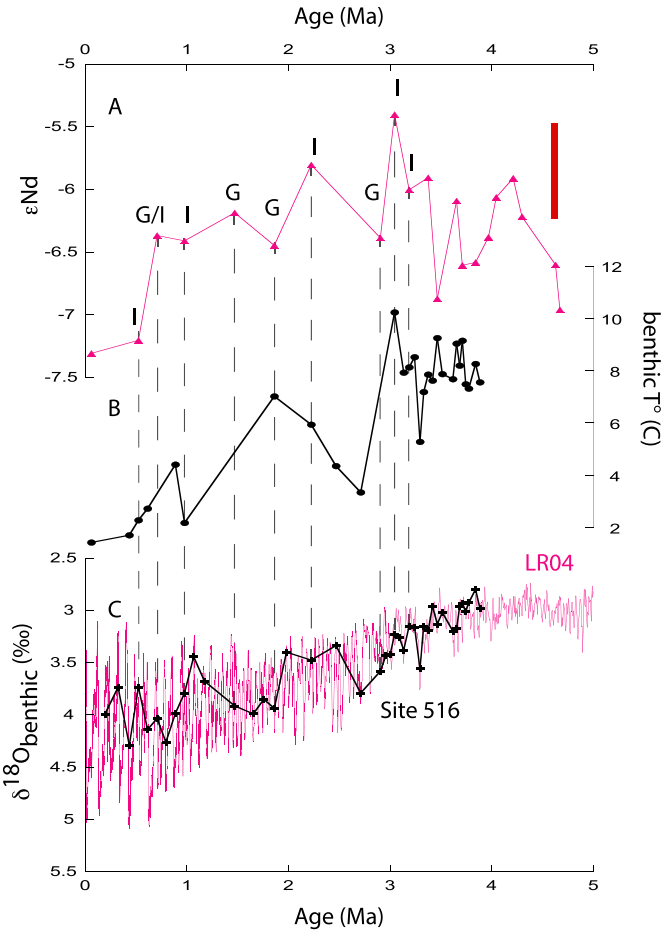

Fig. 4. Identifying glacial, interglacial and data point in between. a) Foraminiferal εNd from Site 516 (red). b) benthic (*U. peregrina)* Mg/Ca-derived temperatures from Site 516 (black). c) benthic (mixed *U. peregrina and C. wuellerstorfi*) $\delta^{18}O$ record from Site 516 (black) and global benthic LR04 stack (Lisiecki and Raymo, 2005; red). I= Interglacial; G = Glacial; G/I = data point in between. Error bar for εNd-values is indicated as red bar. (For interpretation of the references to color in this figure legend, the reader is referred to the Web version of this article.)

At Site 516 we see significant changes in εNd over the Plio-Pleistocene (~2 εNd-units, Fig. 4a). During the warm Pliocene interval between 4.7 and 3.0 Ma, we observe a trend toward higher εNd-values, with maximum values of about −5.5 at ~3 Ma (Fig. 4a). Over the last 3 million years, Site 516 εNd-values become markedly lower, reaching the '*modern-property*' AAIW values of −7.3. Our Plio-Pleistocene trend over the last 3 Ma signals important water provenance changes occurring coeval with major global climatic changes, including the onset of Northern Hemisphere Glaciation and global cooling (Fedorov et al., 2013; Lisiecki and Raymo, 2005; Mudelsee and Raymo, 2005).

A recent study (Howe et al., 2016) of the last glacial/interglacial from the same region (the Brazil margin) and similar depths found a range of values of slightly more than ~1 εNd unit, which is about half of the change we observe across the Plio-Pleistocene. Thus, given that the temporal resolution of our study does not resolve glacial-interglacial periods, we carefully examined the time period represented by single data points to determine if these εNd data (also using BWT in Fig. 4b for comparison) are within glacials, interglacials or are in between, in order to rule out a possible bias through the selection of samples.

Our low sedimentation rates over the last 3 million years means

that each εNd sample (2 cm) integrates a minimum average time period of ~5 ka. Due to bioturbation and occasional rotary coring disturbance, we estimate on average a time resolution of approximately 5–10 ka. This means our εNd signatures from Site 516 represent average bottom water signals either of interglacials, glacials or are a mixed glacial-interglacial time signal (Fig. 4a).

To infer which intervals our εNd signatures represent, we compared our Site 516 benthic $\delta^{18}O$ record with the global LR04 stack (Lisiecki and Raymo, 2005) (Fig. 4a, c). The comparison with the LR04 stack gives an indication of typical glacial and interglacial values for our εNd signatures within a maximum error of about 100 ka (due to our age model). The comparison with our $\delta^{18}O$ record from the same site has helped to clarify if an εNd value matches with glacials, interglacials or mixed glacial-interglacials (Fig. 4a, c). The comparisons show that the εNd signatures represent a good mix of glacials/interglacials over the critical time period 0–3 Ma (Fig. 4a, c). Further, over this critical time period there is on average almost no difference in εNd signatures between glacials (−6.3; 3 data points) and interglacials (−6.2; 4 data points). Hence, although we present a low-resolution εNd record for the last 3 million years, we are confident that it is not significantly biased by over selection of glacial or interglacial time periods. Therefore we propose it is reasonable to interpret our record as reflecting long-term trends.

3.2. Reconstruction of the provenance of bottom waters over the Plio-Pleistocene using εNd signatures

To explore contributions from Southern Ocean, North Atlantic and Pacific water mass sources, we compare our Site 516 εNd record with deep-sea ferromanganese crusts from other sites tracking water masses at depths below AAIW, namely CDW in the Atlantic, Pacific, and Indian Ocean sectors of the Southern Ocean, NADW (discussed in section 3.6) and Central Pacific Waters (Figs. 1 and 5;

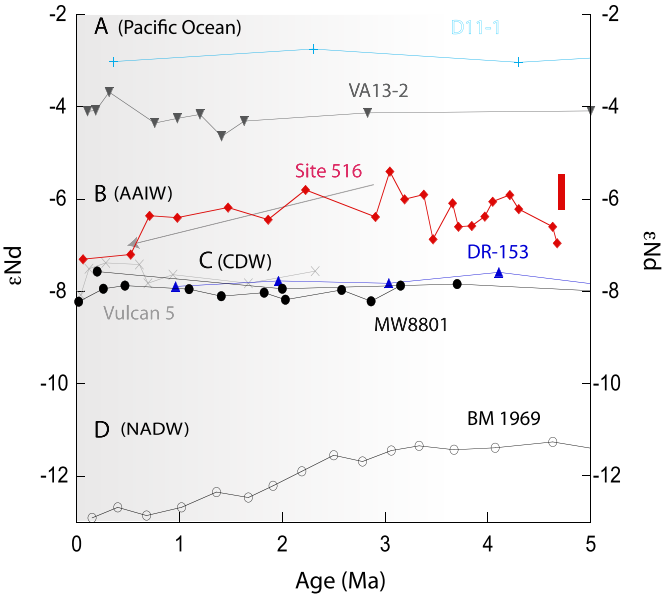

Fig. 5. Plio-Pleistocene Fe-Mn-oxide encrusted foraminiferal εNd from Site 516 in comparison with other coeval ferromanganese crust εNd data from different ocean basins. a) εNd from west and central Pacific crusts D11-1 (light blue; Ling et al., 1997, 1800 m water depth) and VA13-2 (gray; Abouchami et al., 1997; 4800 m water depth). b) Foraminiferal εNd from Site 516 (red), within the present influence of AAIW. c) εNd crust records from the deep Southern Ocean (all from Frank et al., 2002): Vulcan 5 (light gray; water depth: 3690–3900 m), DR-153 (blue; 3300-3150 m water depth) and MW8801 (black; 3993 m water depth). d) εNd crust data from the North Atlantic: BM1969 (Burton et al., 1997, 1829 m water depth). The shaded area indicates the time interval of the development of modern- AAIW. (For interpretation of the references to color in this figure legend, the reader is referred to the Web version of this article.)

and Frank et al., 2002; Ling et al., 1997; Burton et al., 1997; Abouchami et al., 1997). Values from the North Atlantic and Pacific crusts serve to constrain long-term changes in endmembers as each data point represents an average value over longer time periods. For instance, each data point from Vulcan 5 represents 81 kyr (Frank et al., 2002) and individual data points from other sites may represent several 100 s kyr (Frank et al., 2002; Ling et al., 1997). In case of site VA13-2 some data values integrate over up to 1.6 Myr (Abouchami et al., 1997).

The Southern Ocean Fe-Mn crust records are located close to the polar front where watermasses of different ocean basins mix to form a homogenous CDW end member signal (Frank et al., 2002; Stichel et al., 2012). They show εNd-values for CDW of −7 to −8 throughout the time interval between 4.7 Ma and today (Fig. 5c; Frank et al., 2002) suggesting that the time-integrated signal in these deep Southern Ocean areas remained rather constant.

The comparison of the CDW records and the intermediate depth waters at Site 516 documents pronounced differences between their εNd-values between 4.7 and 3 Ma, with Site 516 values higher by ~2.5 or so εNd-units at ~3 Ma (Fig. 5b and c; Frank et al., 2002). These conditions change after 3 Ma when εNd-values at Site 516 start to become more negative, reaching modern values and simultaneously converging on CDW values over the last ~500 ka (Fig. 5b and c). The similarity of εNd-values of AAIW and CDW in the present-day reflects the extensive mixing of waters in the Southern Ocean where AAIW is formed (Stichel et al., 2012). There, CDW waters almost reach the surface, leading to an almost homogenous εNd signature from subsurface to abyssal depths (Piepgras and Wasserburg, 1982; Stichel et al., 2012). Hence, we interpret the evolution of εNd-values at Site 516 after 3 Ma, culminating in the convergence with CDW values near 500 ka, as the result of strengthened mixing and upwelling near the Polar Front down to CDW depths.

Between 4.7 and 3.0 Ma, the distinct difference in the εNd-values of CDW, as reflected by the Fe-Mn crusts and the more positive εNd-values of 'proto-AAIW' at Site 516 (Fig. 5b and c), means that these mixing processes were significantly reduced or absent, and instead the proto-AAIW was formed in a more stratified water column in the Southern Ocean. The more positive εNd-values in the intermediate water indicates that Pacific-derived water was overlying CDW. The offset of the εNd records shows Site 516 εNd-values as high as −5.5, CDW εNd-values of −7 to −8 (Frank et al., 2002), and Central Pacific εNd-values of −3 to −4 (Ling et al., 1997; Abouchami et al., 1997, Fig. 5a, b, c). During these times we speculate that Pacific waters entered the southwest Atlantic at shallower depths through the Drake Passage without (or with minor) deep upwelling of CDW. Hence, AAIW with a deep CDW source, as we know it today, did not yet exist in the southern Atlantic Ocean prior to 3 Ma. The only exceptions before this time at Site 516 are the relatively negative εNd-values of −7 at ~3.4 Ma and ~4.7 Ma. These episodes showing low εNd may suggest deeper mixing of CDW at the Pacific Polar Front, as during the time period around 2–3 Ma. However, these changes were short-lived and not sufficient to reach a modern-property CDW signature.

3.3. External εNd from eolian dust or Antarctic shelf waters?

One possible explanation for the decreasing Plio-Pleistocene εNd offset between Site 516 and the Circumpolar Fe-Mn crusts in Fig. 5b and c (Frank et al., 2002) is addition of external Nd to the subpolar formation area of AAIW. For example, it has been suggested that the εNd of seawater is sometimes changed by dissolution of Nd in eolian dust (Rickli et al., 2010). This option, however is unlikely at Site 516. First, AAIW is formed in the open ocean far from large continental dust source areas. Second, during the

present-day and the last few glacial cycles Antarctic dust and Patagonian sediments/dust show much more positive εNd-values of −4 to +1 (e.g. Delmonte et al., 2008 and refs. therein). As the atmospheric wind circulation strengthened from the warm Pliocene towards the cooler Pleistocene (Brierley et al., 2009), we would expect a trend to more positive values during this time, which is opposite to the pattern we observe.

Similarly, a significant addition of εNd from Antarctic shelf waters is an unlikely explanation for the observed Plio-Pleistocene trend toward more negative εNd. Present-day shelf waters around Antarctica are highly variable (with εNd between +2 and −27 from West to East Antarctica; Lambelet et al., 2018); this variability is homogenized by vigorous mixing within the Antarctic Circumpolar Current and practically does not reach CDW, which is the main source of present-day AAIW (Carter et al., 2012). CDW in the Southern Ocean shows very homogenous values of −8 to −9 (Carter et al., 2012; Stichel et al., 2012; Lambelet et al., 2018) comparable to the Plio-Pleistocene long term εNd crust data from sites in the deep Southern Ocean (Frank et al., 2002, Fig. 5c).

Also during the warm Pliocene, it is difficult to reconcile northward subduction of a radiogenic εNd signal from the Antarctic shelf towards the intermediate waters at Site 516. The northward transport of such a signal from the far south would be difficult due to the reduced westwind strength (e.g. Brierley et al., 2009). Hence, the more straightforward explanation for our observed more radiogenic εNd during the Pliocene is a simple inflow of more radiogenic Pacific water masses with minor upwelling of CDW.

3.4. A comparison with opal MAR from Site 745

The shift from more stratified waters towards greater upwelling of CDW in the Southern Ocean over the last ~3 Ma, indicated by the Site 516 εNd record, is supported by an Opal MAR record from Australian-Antarctic Basin Site 745 (Fig. 6a and b). This site is presently located south of the Polar Front in the Southern Ocean (60°S, 86°E; for location see Fig. 1) where upwelling of CDW reaches the near-surface (Billups et al., 2013). High opal burial flux values can be interpreted to record greater surface productivity related to upwelling of nutrient-rich CDW. Opal production at this site is not affected by sea ice formation (in contrast to Antarctic Site 1096) as this site is currently mostly located within ice-free waters (Billups et al., 2013 and refs therein). Hence we interpret this Opal MAR record as a proxy for upwelling of CDW south of the Polar Front (Anderson et al., 2009; Billups et al., 2013). During the Pliocene when our εNd from Site 516 show high values, the deeper Site 745 Opal MAR values reflect reduced upwelling prior to 3 Ma (Fig. 6a and b). During these times high diatom productivity and related upwelling was restricted to regions near the coast of the Antarctic continent (Cortese et al., 2004; Hillenbrand and Cortese, 2006; Billups et al., 2013). During the Plio-Pleistocene, after about 3 Ma, our Site 516 εNd data exhibit more negative values consistent with greater CDW influence, and Site 745 Opal MAR values increase, suggesting increased upwelling of nutrient-rich CDW south of the present Polar Front (Fig. 6a and b).

3.5. Emergence of AAIW water temperatures and salinity

BWT and salinities ($\delta^{18}O_{IVC\text{-}seawater}$) from Site 516 complete the picture of oceanographic changes in the Southern Ocean and the development of modern-property cold, fresh AAIW (Fig. 6c and d). Our Site 516 *U. peregrina* temperature record shows a good agreement with our mixed species temperature record (*C. wuellerstorfi* or *U. peregrina*) from Site 516A during the time period of overlap (~4–2.8 Ma; Fig. 6d) suggesting acceptable reproducibility between species and Holes. Prior to 3 Ma, bottom waters at this Site (1313 m)

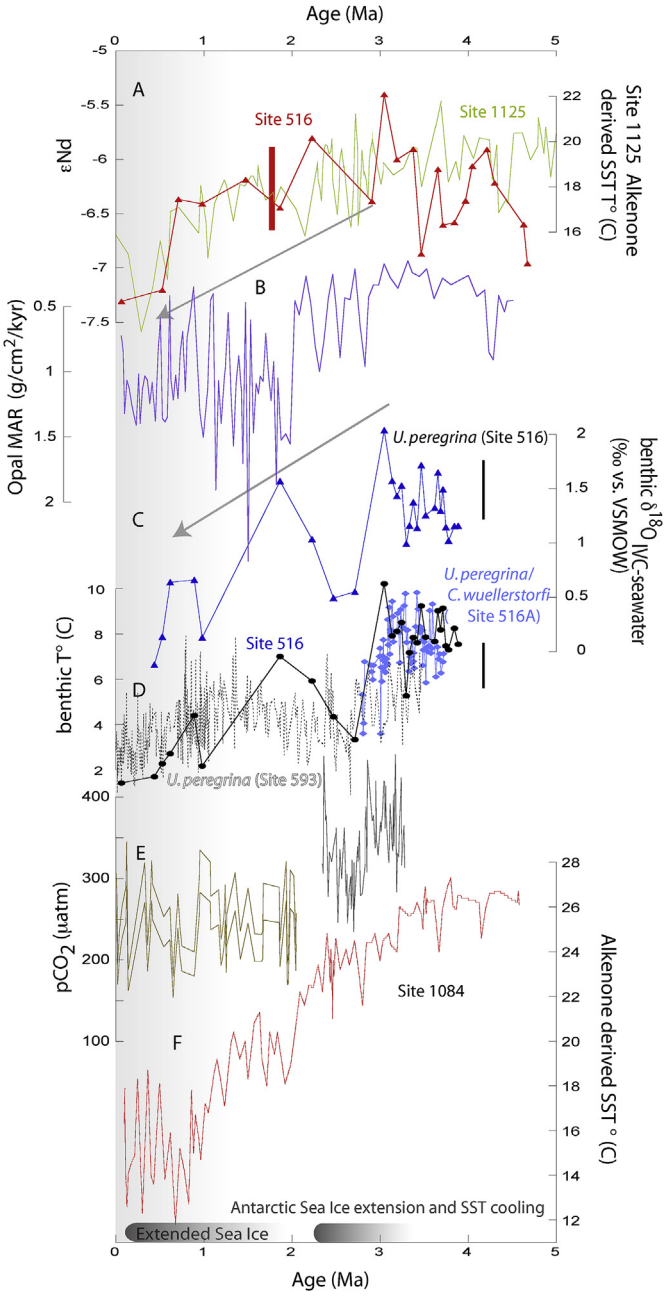

Fig. 6. Proxy data from different Sites during the Plio-Pleistocene. a) Fe-Mn encrusted foraminiferal εNd from Site 516 (red) and alkenone-derived SST from Site 1125 (light gray; Herbert et al., 2016). b) Opal MAR from Site 745 (purple; see methods for details). c) Benthic $\delta^{18}O_{IVC\text{-}seawater\text{-}values}$ from Site 516 (blue) d) Benthic (*U. peregrina*) $T_{Mg/Ca}$ from Site 516 (black), mixed benthic (*U. peregrina* and *C. wuellerstorfi*) $T_{Mg/Ca}$ from Site 516A (blue) and benthic (*U. peregrina*) $T_{Mg/Ca}$ from Pacific Site 593 (McClymont et al., 2016; dotted line). e) Atmospheric CO_2 reconstruction based on foraminiferal boron isotopes (Hoenisch et al., 2009; Martinez-Boti et al., 2015). During ~2-0 Ma: light gray (35), minimum and maximum estimations; During ~3.3–2.3 Ma: gray (36). f) Alkenone-derived sea surface temperature changes from Benguela upwelling Site 1084 (Marlow et al., 2000; red). Error bars are indicated (see methods). Timings of Antarctic sea ice extension are indicated. (For interpretation of the references to color in this figure legend, the reader is referred to the Web version of this article.)

were ~7–10 °C, or roughly 5–6 °C warmer than modern values (~3 °C; Locarnini et al., 2010). After 3 Ma, BWT decreases and modern BWT are attained only by 1.0–0.5 Ma (Fig. 6d). Our reconstructed $\delta^{18}O_{IVC\text{-}seawater}$-values indicate more saline bottom

water conditions prior to 3 Ma (Fig. 6c). Along with AAIW cooling, decreasing εNd-values, and increasing Opal MAR at Site 745 after 3 Ma, our Site 516 benthic $\delta^{18}O_{IVC\text{-}seawater}$ values further indicate a pronounced freshening of ~1‰ (Fig. 6a,b,c,d) after this time.

The warmer and more saline Atlantic intermediate waters prior to 3 Ma support our interpretation of reduced vertical mixing and upwelling of CDW near the Polar Front and a direct inflow of Pacific-sourced intermediate water, resulting in a warmer, more saline proto-AAIW than today (Fig. 7a). After 3 Ma, Atlantic intermediate waters became cooler and fresher which we interpret to reflect a gradual emergence of modern-property AAIW due to increased vertical mixing near the Polar Front (Fig. 7b).

Global paleoceanographic records support this view. Pliocene alkenone-derived sea surface temperature (SST) reconstructions from the mid-latitudes of the South Atlantic and Pacific oceans (Sites 1125, 1090 and 1088; Herbert et al., 2016; Martinez-Garcia et al., 2010) document SSTs that were 5–6 °C warmer than today. Southern Hemisphere westerly wind speeds were significantly reduced at the Subantarctic Front at southeast Atlantic ODP Sites 1091 and 1090 (Hillenbrand and Cortese, 2006; Martinez-Garcia et al., 2011). Model simulations also suggest reduced subtropical and subpolar zonal atmospheric streamflow associated with reduced Pliocene temperature gradients between the poles and the tropics and widely expanded tropics and subtropics (Brierley et al., 2009; Fedorov et al., 2013). Consequently, northward Ekman transport of proto-AAIW waters, which is driven by the westerlies, would have been considerably weakened during the warm Pliocene as well.

The warmer, saltier properties of Pliocene AAIW are consistent with Antarctic sea ice proxy records. Sediment core AND-1B from beneath the Ross Ice Shelf indicates distinctly less sea ice (based on ice diatoms), and warmer sea surface conditions of ~2–4 °C (based on TEX SST) during the warm Pliocene (McKay et al., 2012, location is in Fig. 1). Less sea ice is also indicated by high amounts of biogenic opal in Antarctic ODP Sites 1096 and 1095 (Hillenbrand and Cortese, 2006). This less sea ice was simulated to reduce upwelling of CDW in the Southern Ocean (Hill et al., 2017). Consequently, the warmer, reduced Antarctic sea ice extent conditions during the Pliocene were not favorable for producing modern-property AAIW (Evans et al., 2018; Pellichero et al., 2018). Today, seasonal advances and retreats of sea ice are working as a circulator pump promoting upwelling of CDW and the formation of relatively fresh and cold AAIW (Evans et al., 2018; Pellichero et al., 2018). The relative freshness of AAIW is thereby mostly due to seasonal melting of sea ice (Pellichero et al., 2018; Evans et al., 2018) which can be expected to be almost absent during warm Pliocene conditions. Hence, we can explain our observations of more saline intermediate water conditions at Site 516 during the Pliocene compared to the Pleistocene. Additionally, the reduced northward circulation of these intermediate waters towards Site 516 might have resulted in an increased imprint of the surrounding more saline South Atlantic waters.

3.6. Tracing southern-sourced intermediate waters at Site 516: evidence from εNd, Mg/Ca bottom temperatures, and salinity changes

Together with our bottom temperature and salinity reconstructions, we also can constrain that we are not monitoring regional shallower (sub-) surface waters at Site 516 and/or deeper NADW from the north. Between 4 and 3 Ma, bottom temperatures and salinities are high (8-10 °C; 1–1.5‰) and εNd-values are high (up to −5.5; Fig. 6a,c,d). Whereas high temperatures and high salinities are compatible with a greater influence of regional shallow waters, the high εNd-values are inconsistent with this scenario and rather suggest a Pacific source. Shallow waters (~500 m water depth) near Site 516 in the present-day show very low εNd-values of −12 (Wu, 2019), even more negative than the Circumpolar Fe-Mn crusts. These negative shallow water εNd-values reflect input of Nd from regional continental sources and can be expected to persist as sources of shallow water εNd signatures through the entire time period.

During the Plio-Pleistocene cooling interval between 3 and 0 Ma, the trend toward more negative εNd-values at Site 516 could also be interpreted to indicate an increased influence of NADW waters from below. Similar trends, for example, are seen at Site 516 and in the North Atlantic record of Fe-Mn crust BM1969 (Fig. 5b,d; and Burton et al., 1997), which is bathed in NADW. However, our reconstructed bottom salinities at Site 516 show a pronounced freshening, which is in clear contrast to increased NADW influence, as NADW is a saline water mass, significantly more saline than AAIW. Hence, most likely we observe two developments that have taken place independently since ~3 Ma. In the Southern Ocean, there is an increased vertical mixing of less radiogenic CDW and the onset of the modern-property fresh and cold AAIW. In the North Atlantic, the trend to more negative εNd signatures likely reflects an endmember change of εNd of NADW. The amplified Northern Hemisphere Glaciation increased contributions from Archean and Proterozoic shield regions surrounding the North Atlantic basin (Frank et al., 2002). Increased weathering and amplified input of such detritus into the North Atlantic would result in more negative εNd.

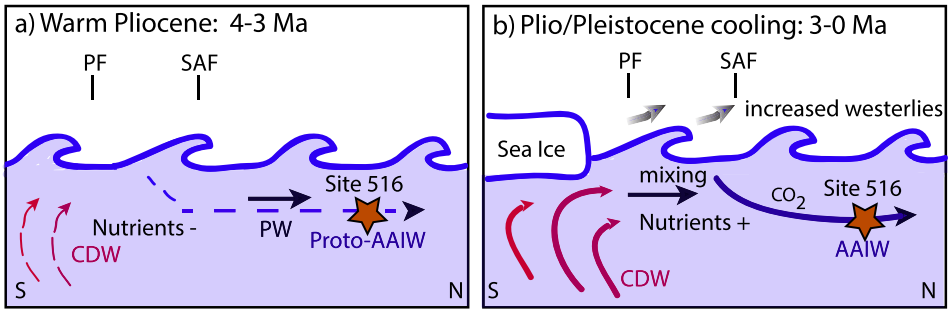

Fig. 7. Schematic overviews of the formation of AAIW during the Plio-Pleistocene. a) The situation during the warm Pliocene (4-3 Ma), with more stratified waters near the Polar Front, overflow of Pacific Waters (PW) into the South Atlantic Ocean, and warmer and more saline proto-AAIW. Contributions from Circumpolar Deep Water (CDW) were low or absent. b) The development of modern cooler and fresher AAIW during the last 3 Ma, with the onset of deep vertical mixing and upwelling of nutrient rich CDW near the Polar Front and increased uptake of atmospheric CO_2. The drawings are based on information of this and other studies (Sarmiento et al., 2004; McKay et al., 2012; Hill et al., 2017; Martinez-Garcia et al., 2011) Site 516 is indicated with a red star. PF= Polar front. SAF= Subantarctic Front. (For interpretation of the references to color in this figure legend, the reader is referred to the Web version of this article.)

Our conclusion that the εNd-values of Site 516A mainly reflect a signal from the South Pacific or the Southern Ocean is further supported by a comparison with an alkenone-derived SST from Southwest Pacific ODP Site 1125 (Fig. 6a; Herbert et al., 2016). Our εNd-values show a good accordance with alkenone-derived SST over the Plio-Pleistocene. The location of Site 1125 (42°S, shown in Fig. 1) is close to the Subtropical Front, which is the northern limit for subantarctic waters, and therefore likely to show sensitivity to climate changes in the Southern Ocean. Especially before 3 Ma, when temperatures at Site 1125 are high, Site 516 shows higher εNd-values. Conversely, when SST from Site 1125 shows a distinct cooling trend after 3 Ma, εNd-values from Site 516 show a similar decreasing trend (Fig. 6a; Herbert et al., 2016). These relationships make sense, because with colder temperatures in middle-to-high southern latitudes during the Plio-Pleistocene there was a greater temperature difference between low and high latitudes, causing stronger westerlies (Brierley et al., 2009; Fedorov et al., 2013). Along with significantly increased Antarctic sea ice compared to the warm Pliocene, this in turn would enhance deep vertical mixing in the Southern Ocean (McKay et al., 2012; Hill et al., 2017; Evans et al., 2018; Pellichero et al., 2018). This could explain how the more negative εNd-values of CDW could be entrained into AAIW and transported towards Site 516. This hypothesis also allows for the short intervals at around 3.4 and 4.7 Ma, when relatively low εNd-values at Site 516 seem to occur at the same time as lower temperatures at Site 1125 (Fig. 6a; Herbert et al., 2016).

3.7. Global cooling and the role of AAIW for atmospheric CO_2

Major global cooling began ~2 million years earlier than the development of modern AAIW in the Atlantic Ocean. Its effects included increased meridional surface ocean temperature differences, cooling of surface waters at subtropical upwelling regions in the Northern and Southern Hemispheres, and shoaling of the equatorial east Pacific thermocline, leading to the establishment of a temperature difference between the east and west Pacific (Fedorov et al., 2013; Steph et al., 2010). This time difference supports previous studies indicating that a climate threshold was reached at ~3 Ma, with increased Antarctic sea ice cover, meridional temperature gradients, and invigorated Southern Ocean geostrophic circulation (McKay et al., 2012; Hill et al., 2017), culminating in the emergence of modern-property AAIW in the Atlantic Ocean. This is expressed by colder and fresher AAIW, and converging εNd-values towards CDW water masses at Site 516 (Fig. 5b and c; 6c,d). The influence of inflow of warmer and more saline intermediate Pacific-sourced water diminished, and instead enhanced deep vertical mixing at the Polar Front in the Pacific sector emerged. This and increased subduction of fresh and cold waters at the Polar Front resulted in fresher and colder conditions.

The cooling trend that followed during the Plio-Pleistocene, recorded by intermediate water masses in the Atlantic Ocean, is not limited to the Atlantic, as a similar trend (inferred from benthic *U. peregrina* Mg/Ca) has been observed in the southwest Pacific at DSDP Site 593 (McClymont et al., 2016, Figs. 1a and 6d). This indicates that modern AAIW circulation likely started to develop in both ocean basins, however slightly earlier at Site 593 at ~3.3 Ma (McClymont et al., 2016). However, that study did not reconstruct source water changes at the formation region of AAIW and therefore it still has to be determined whether deep vertical mixing started there at the same time. The AAIW cooling trend at Site 516 is synchronous with a pronounced sea surface cooling of up to ~10 °C at South Atlantic Benguela upwelling Sites 1082 (Etourneau et al., 2009) and 1084 (Marlow et al., 2000, Fig. 6d, f). Today, the Benguela Current is ventilated by 4 SV (1 SV = 10^6 m^3s^{-1}) AAIW and South Atlantic Mode Waters that supply subsurface nutrients to this highly-productive upwelling system (Gordon et al., 1992; Marlow et al., 2000 and ref. therein). Hence, our Site 516 record is the first direct proxy evidence for Atlantic AAIW, which shows how cooled intermediate waters were transported towards the Benguela region. These cold subsurface waters were then brought to the surface when atmospheric circulation and coastal upwelling strengthened (Marlow et al., 2000; Etourneau et al., 2009, 2012).

The gradual development of upwelling of nutrient rich CDW in the Southern ocean, and modern-property AAIW formation beginning at ~3 Ma, which previously was fed by warmer and more saline intermediate waters from the South Pacific, is reflected in Site 516 by a trend towards more negative εNd-values, along with cooling and freshening and supported by an increase in Opal MAR at Site 745 (Fig. 6a–d). This evolution is coeval with significant long-term reductions of atmospheric CO_2, as indicated by reconstructions of boron isotopes from deep sea sediment cores (e.g. Hoenisch et al., 2009; Martinez-Boti et al., 2015, Fig. 6a–e). We suggest that the development of present-day-like AAIW over this time interval, with enhanced deep vertical mixing of water masses near the Polar Front, was not only a reaction to global cooling, but also a driver for coeval global CO_2 reduction (see Fig. 6e; Hoenisch et al., 2009; Martinez-Boti et al., 2015).

At ~3 Ma, when the modern development of AAIW began with significant surface cooling in the Southern Hemisphere mid-to high latitudes (Martinez-Garcia et al., 2010; McKay et al., 2012; Herbert et al., 2016), the colder water (up to 5 °C) could uptake significantly more CO_2 into the ocean than the warmer precursor. This is because atmospheric CO_2 has a higher solubility in colder water. This short-term trapped atmospheric CO_2 could then be sequestered in the deep ocean for long time periods (on kyr to myr time-scales). The colder AAIW would have transported the carbon, along with nutrients, to (sub)tropical upwelling regions, fuelling primary productivity and export production (burial of Corg) there (Cortese et al., 2004; Etourneau et al., 2012). Indeed, a bloom of diatoms (through increased Si transport) is observed in these regions during 3-2 Ma, which has been suggested to be effective for decreasing atmospheric CO_2 levels (Cortese et al., 2004; Etourneau et al., 2012). At the same time the increased ice cover close to Antarctica (McKay et al., 2012) would have reduced direct outgassing of oceanic CO_2 through upwelling of CDW close to the Antarctic continent (Hillenbrand and Cortese, 2006; Etourneau et al., 2012). Also, the subarctic North Pacific was more stratified, which further hindered the escape of sequestered carbon (Sigman et al., 2004). In addition, increased primary productivity (mosty diatoms) in the Southern Ocean would have further decreased the atmospheric CO_2 levels during the Quaternary (Fig. 6b; Billups et al., 2013). Other effects, such as increased aeolian Fe input after 2.6 Ma through increased westerlies, would have contributed additional support to the productivity increase and CO_2 uptake into the Southern Ocean (Billups et al., 2013; Martinez-Garcia et al., 2011).

4. Conclusions

We document the emergence of modern-property AAIW during the Plio-Pleistocene in the South Atlantic Ocean at DSDP Site 516. Using a multi proxy-approach, including εNd in Fe-Mn-oxide encrusted foraminifera, benthic foraminiferal $BWT_{Mg/Ca}$, and stable isotopes, we reconstruct AAIW source water provenance, temperature, and salinity changes.

Our results indicate that prior to Northern Hemisphere Glaciation, during the Pliocene warm interval between 4 and 3 Ma, modern-property AAIW (cold, fresh, and εNd similar to CDW) did not exist in the South Atlantic Ocean. Instead, higher (more Pacific-like) εNd-values at Site 516, compared with deeper samples bathed in CDW in the Southern Ocean, document more stratified

conditions near the Polar Front at that time, with direct inflow of Pacific waters to the intermediate depth southwestern Atlantic (Fig. 7a). At this time, Atlantic intermediate waters were 6 °C warmer and more saline.

The emergence of modern-property AAIW occurred gradually during the last ~3 million years, evidenced at Site 516 by cooling and freshening and an εNd trend away from Pacific-like values, converging on values consistent with CDW (decreasing by ~2 units). These changes reflect the onset of deep vertical mixing of water masses in the source region of AAIW near the Polar Front, which were transported northward and most likely contributed to cooling of subtropical upwelling regions (Fig. 7b). These observations are in agreement with recent model simulation studies indicating polar cooling, amplified meridional temperature gradients, stronger Southern Ocean geostropic flow, and greater CPW upwelling and entrainment (Hill et al., 2017). The development of modern AAIW with upwelling of nutrient rich CDW close to its source region likely facilitated increased CO_2 storage of the ocean and thus accelerated the global climate changes towards Pleistocene icehouse conditions.

Author contributions

C.K. performed the analyses and wrote the first draft. All authors were involved in interpreting the data and bringing the manuscript to completion.

Conflicts of interest

The authors declare no competing interests.

Data and materials availability

Data is available at the NOAA National Center for Environmental Information (https://www.ncdc.noaa.gov/paleo/study/27750).

Acknowledgments

We thank the IODP for providing sample material. For technical support in the lab we thank L. Bolge. For further help in the lab and discussions we thank Y. Wu, W. Huang, K. Esswein, A. Dial, G. B. Whitlock, Y. Kiro, M. Yehudai, A. Bahr and D. Nürnberg. We thank the Max Kade Foundation, the German Research Foundation (project: KA3461/1-2), Columbia's Center for Climate and Life, and the Storke Endowment of the Columbia Department of Earth and Environmental Sciences for financial support for C.K. This is LDEO contribution number 8355.

Appendix A. Supplementary data

Supplementary data to this article can be found online at https://doi.org/10.1016/j.quascirev.2019.105945.

References

Abernathey, R.P., et al., 2016. Water-mass transformation by sea ice in the upper branch of the Southern Ocean overturning. Nat. Geosci. 9, 596–601.
Abouchami, W., et al., 1997. Secular changes of lead and neodymium in central Pacific seawater recorded by a Fe-Mn Crust. Geochem. Cosmochim. Acta 61, 3957–3974.
Abbott, A., et al., 2015. Bottoms up: sedimentary control of the deep North Pacific Ocean's epsilon-Nd signature. Geology 43 (11), 1035-1035. https://doi.org/10.1130/G37114.1.
Anderson, R.F., et al., 2009. Wind-driven upwelling in the Southern ocean and the deglacial rise in atmospheric CO_2. Science 13, 1443–1448.
Antonov, J.I., et al., 2010. World ocean Atlas 2009, volume 2: salinity. In: NOOA Atlas NESDIS 69 S. Levitus. U.S. Gov. Printing Office.
Barash, M.S., et al., 1983. Quaternary biostratigraphy and surface Paleotemperatures based on planktonic foraminifers. In: Barker, P.F., Carlson, R.L., Johnson, D.A. (Eds.), Deep Sea Project. U.S. Government Printing Office, pp. 849–869. Initial Reports, 72.
Barker, P.F., et al., 1983. Site 516: Rio Grande Rise, Init. Repts. DSDP, vol. 72. US Government Printing Office, 1983.
Barker, S., Greaves, M., Elderfield, H., 2003. A study of cleaning procedures used for foraminiferal Mg/Ca paleothermometry. Geochem. Geophys. Geosyst. 4 (9), 8407. https://doi.org/10.1029/2003GC000559.
Barron, J.A., Larsen, B., 2005. Shipboard Scientific Party (2005): Moisture and Density Measured on ODP Hole 119-745B. PANGAEA. https://doi.org/10.1594/PANGAEA.258288.
Berggren, W.A., Aubry, M.P., Hamilton, N., 1983. Neogene magnetobiostratigraphy of deep sea drilling project Site 516. In: Barker, P.F., et al. (Eds.), Deep Sea Project, Initial Reports, vol. 72. U.S. Government Printing Office, pp. 675–713. https://doi.org/10.2973/dsdp.proc.72.130.1983.
Billups, K., Aufdenkampe, A., Hays, R., 2013. Late Miocene through early Pleistocene nutrient utilization and export production in the Antarctic zone of the Southern ocean. Glob. Planet. Chang. 100, 353–361.
Bishop, S.P., et al., 2016. Southern ocean overturning compensation in an eddy-resolving climate simulation. J. Phys. Oceanogr. 46, 1575–1592. https://doi.org/10.1175/JPO-D-15-0177.1.
Brierley, C.M., et al., 2009. Greatly expanded tropical warm pool and weakened Hadley circulation in the early Pliocene. Science 323, 1714–1718.
Burton, K.W., et al., 1997. Closure of the central American isthmus and its effect on deep-water formation in the north- Atlantic. Nature 386, 382–385.
Carter, P., et al., 2012. The neodymium isotopic composition of waters masses in the eastern Pacific sector of the Southern Ocean. Geochem. Cosmochim. Acta 79, 41–59.
Cortese, G., et al., 2004. Opal sedimentation shifts in the world Ocean over the last 15 Myr. Earth Planet. Sci. Lett. 224, 509–527.
de Boer, B., et al., 2014. Persistent 400,000-year variability of Antarctic ice volume and the carbon cycle is revealed throughout the Plio-Pleistocene. Nat. Commun. 5, 2999. https://doi.org/10.1038/ncomms3999.
Delmonte, B., et al., 2008. Aeolian dust in East Antarctica (EPICA-Dome C and Vostok): provenance during glacial ages over the last 800 kyr. Geophys. Res. Lett. 35, L07703. https://doi.org/10.1029/2008GL033382.
Du, J., Haley, B.A., Mix, A.C., et al., 2016. Neodymium isotopes in authigenic phases, bottom waters and detrital sediments in the Gulf of Alaska and their implications for paleo-circulation reconstruction. Geochem. Cosmochim. Acta 193, 14–35.
Duplessy, J.-C., et al., 1984. ^{13}C record of benthic foraminifer in the last interglacial ocean: implications for the carbon cycle and the global deep water circulation. Quat. Res. 21, 225–243.
Ehrmann, W., Grobe, H., 1991. Cyclic sedimentation at sites 745 and 746. In: Barron, J., Larsen, B., et al. (Eds.), Proceedings of the Ocean Drilling Program, Scientific Results, vol. 119. Ocean Drilling Program, College Station, TX, pp. 225–237. Data at. https://doi.org/10.1594/PANGAEA.51491.
Elderfield, H., et al., 2006. Calibrations for benthic foraminiferal Mg/Ca paleothermometry and the carbonate ion hypothesis. Earth Planet. Sci. Lett. 250, 633–649.
Elderfield, H., et al., 2010. A record of bottom water temperature and seawater $\delta^{18}O$ for the Southern Ocean over the past 440 kyr based on Mg/Ca of benthic foraminiferal Uvigerina spp. Quat. Sci. Rev. 29 (1–2), 160–169.
Elmore, A.C., et al., 2015. Antarctic Intermediate Water properties since 400ka recorded in infaunal (Uvigerina peregrina) and epifaunal (Planulina wuellerstorfi) benthic foraminifera. Earth Planet. Sci. Lett. 428, 193–203.
Elmore, A.C., et al., 2011. Testing the extraction of past seawater Nd isotopic composition from North Atlantic deep sea sediments and foraminifera. Geochem. Geophys. Geosyst. 12 (9). https://doi.org/10.1029/2011GC003741.
Etourneau, J., et al., 2009. Pliocene–Pleistocene variability of upwelling activity, productivity, and nutrient cycling in the Benguela region. Geology 37, 871–874.
Etourneau, J., et al., 2012. Contributions of changes in opal productivity and nutrient distribution in the coastal upwelling systems to Late Pliocene/Early Pliocene climate cooling. Clim. Past. 8, 1435–1445.
Evans, D., et al., 2016. Planktic foraminifera shell chemistry response to seawater chemistry: Pliocene-Pleistocene seawater Mg/Ca, temperature and sea level change. Earth Planet. Sci. Lett. 438, 139–148.
Evans, D.G., et al., 2018. The cold transit of Southern ocean upwelling. Geophys. Res. Lett. 45. https://doi.org/10.1029/2018GL079986.
Fedorov, A.V., et al., 2013. Patterns and mechanisms of early Pliocene warmth. Nature 496, 43–49.
Frank, M., et al., 2002. North Atlantic deep water export to the Southern ocean over the past 14 Myr: evidence from Nd and Pb isotopes in ferromanganese crusts. Paleoceanography 17, 12-1 to 12-9.
Garcia, H.E., et al., 2010. World ocean Atlas 2009, volume 4: nutrients (phosphate, nitrate, silicate). In: Levitus, S. (Ed.), NOOA Atlas NESDIS 70. U.S. Gov. Printing Office.
Gordon, A.L., et al., 1992. Thermocline and intermediate water communication between the south Atlantic and Indian oceans. J. Geophys. Res. 97, 7223–7240.
Gruber, N., et al., 2009. Oceanic sources, sinks, and transport of atmospheric CO_2. Glob. Biogeochem. Cycles 23, GB1005. https://doi.org/10.1029/2008GB003349.
Hill, D., Bolton, K.P., Haywood, A.M., 2017. Modelled ocean changes at the Plio-Pleistocene transition driven by Antarctic ice advance. Nat. Commun. 8, 14376.
Hillenbrand, C.D., Cortese, G., 2006. Polar stratification: a critical view from the Southern Ocean. Palaeogeogr. Palaeoclimatol. Palaeoecol. 242 (3), 240–252.

Howe, J.N.W., et al., 2016. Antarctic intermediate water circulation in the South Atlantic over the past 25,000 years. Paleoceanography 31, 1302–1314. https://doi.org/10.1002/2016PA002975.
Hut, G., 1987. Consultants' Group Meeting on Stable Isotope Reference Samples for Geochemical and Hydrological Investigations. Rep. to Dir. Gen., Int. Atomic Energy, Agency, Vienna.
Herbert, T.D., et al., 2016. Late Miocene global cooling and the rise of modern ecosystems. Nat. Geosci. 9, 843–847.
Hoenisch, B., et al., 2009. Atmospheric carbon dioxide concentration across the mid-Pleistocene transition. Science 324, 1551–1554.
Jacobsen, S.B., Wasserburg, G.J., 1980. Sm-Nd isotopic evolution of chondrites. Earth Planet. Sci. Lett. 50, 139–155.
Jeandel, C., 1993. Concentration and isotopic composition of Nd in the south Atlantic Ocean. Earth Planet. Sci. Lett. 117, 581–591.
Karas, C., et al., 2009. Mid-Pliocene climate change amplified by a switch in Indonesian subsurface throughflow. Nat. Geosci. 2, 434–438. https://doi.org/10.1038/NGEO520.
Karas, C., et al., 2017. Pliocene Oceanic Saways and Global Climate, vol. 7. Scientific Reports, p. 39842.
Kraft, S., et al., 2013. Assessment of seawater Nd isotope signatures extracted from foraminiferal shells and authigenic phases of Gulf of Guinea sediments. Geochem. Cosmochim. Acta 121, 414–435. https://doi.org/10.1016/j.gca.2013.07.029.
Lambelet, M., et al., 2018. The neodymium isotope fingerprint of Adélie coast bottom water. Geophys. Res. Lett. 45, 11, 247–11,256. https://doi.org/10.1029/2018GL080074.
Lawrence, K.T., Liu, Z., Herbert, T.D., 2006. Evolution of the eastern tropical Pacific through Plio–Pleistocene glaciation. Science 312, 79–83.
Ling, H.-F., et al., 1997. Evolution of Nd and Pb isotopes in central Pacific seawater from ferromanganese crusts. Earth Planet. Sci. Lett. 146, 1–12.
Lisiecki, L.E., Raymo, M.E., 2005. A Pliocene-Pleistocene stack of 57 globally distributed benthic d18O records. Paleoceanography 20, 1. https://doi.org/10.1029/2004PA001071. PA1003.
Locarnini, R.A., et al., 2010. World ocean Atlas 2009, volume 1: temperature. In: Levitus, S. (Ed.), NOAA Atlas NESDIS 68. US. Government Printing Office, Washington, D.C., p. 184
Lourens, L.J., et al., 2004. Appendix 2.00. In: Gradstein, F.M., et al. (Eds.), A Geologic Time Scale 2004, vol. 2004. Cambridge Univ. Press, Cambridge.
Martin, E.E., Haley, B.A., 2000. Fossil fish teeth as proxies for seawater Sr and Nd isotopes. Geochem. Cosmochim. Acta 64 (5), 835–847. https://doi.org/10.1016/S0016-7037(99)00376-2A.
Martinez-Boti, M.A., et al., 2015. Plio-Pleistocene climate sensitivity evaluated using high resolution CO_2 records. Nature 518 (7537), 49–54, 31.
Martinez-Garcia, A., et al., 2010. Subpolar link to the emergence of the modern equatorial Pacific cold tongue. Science 328, 1550–1553.
Martinez-Garcia, A., et al., 2011. Southern Ocean dust–climate coupling over the past four million years. Nature 467, 312–315.
Marlow, J.R., et al., 2000. Upwelling intensification as part of the Pliocene-Pleistocene climate transition. Science 290, 2288-229.
McCartney, M.S., 1977. In: Angel, M. (Ed.), Subantarctic Mode Water, A Voyage of Discovery. Pergamon, pp. 103–119.
McClymont, E.L., et al., 2016. Pliocene-Pleistocene evolution of sea surface and intermediate water temperatures from the Southwest Pacific. Paleoceanography 31, 895–913.
McKay, R., et al., 2012. Antarctic and Southern ocean influences on late Pliocene global cooling. Proc. Natl. Acad. Sci. 109 (17), 6423–6428, 27.
Mudelsee, M., Raymo, M.E., 2005. Slow dynamics of the northern hemisphere glaciation. Paleoceanography 20, PA4022. https://doi.org/10.1029/2005PA001153.
Osborne, A.H., et al., 2017. The potential of sedimentary foraminiferal rare earth element patterns to trace water masses in the past. Geochem. Geophys. Geosyst. 18, 1550–1568. https://doi.org/10.1002/2016GC006782.
Paillard, D., Labeyrie, L., Yiou, P., 1996. Macintosh program performs time-series analysis. Eos Trans. AGU 77, 379.
Pellichero, V., et al., 2018. The southern ocean meridional overturning in the sea-ice sector is driven by freshwater fluxes. Nat. Commun. 9 https://doi.org/10.1038/s41467-018-04101-2.
Piotrowski, A.M., et al., 2004. Intensification and variability of ocean thermohaline circulation through the last deglaciation. Earth Planet. Sci. Lett. 225 (1), 205–220.
Piotrowski, A.M., et al., 2005. Temporal relationships of carbon cycling and ocean circulation at glacial boundaries. Science 307 (5717), 1933–1938.
Piotrowski, A.M., et al., 2008. Oscillating glacial northern and southern deep water formation from neodymium and carbon isotopes. Earth Planet. Sci. Lett. 272, 394–405.
Piola, A.R., Georgi, D.T., 1982. Circumpolar properties of Antarctic intermediate water and subantarctic mode water. Deep-Sea Res. 29, 687–711.
Piola, A.R., Matano, R.P., 2001. Brazil and Falklands (Malvinas) Currents, vol. 2017. Encyclopedia of Ocean Sciences, pp. 340–349. https://doi.org/10.1006/rwos.2001.0358.
Piepgras, D., Wasserburg, G.J., 1982. Isotopic composition of neodymium in waters from the Drake passage. Science 217, 207–214.
Rickli, J., et al., 2010. Hafnium and neodymium isotopes in surface waters of the eastern Atlantic Ocean: implications for sources and inputs of trace metals to the ocean. Geochem. Cosmochim. Acta 74, 540–557.
Roberts, N.L., et al., 2010. Synchronous deglacial overturning and water mass source changes. Science 327 (5961), 75–78.
Rutberg, R.L., Hemming, S.R., Goldstein, S., 2000. reduced north Atlantic deep water flux to the glacial Southern ocean inferred from neodymium isotope ratios. Nature 405, 935–938.
Sabine, C.L., et al., 2004. The oceanic sink for anthropogenic CO_2. Science 305 (5682), 367–371.
Sarmiento, J.L., et al., 2004. High-latitude controls of thermocline nutrients and low latitude biological productivity. Nature 427, 56–60.
Schlitzer, R., 2012. Ocean Data View. http://odv.awi.de.
Shackleton, N.J., 1974. Attainment of isotope equilibrium between ocean water and the benthonic foraminiferal genus Uvigerina. Isotopic changes in the ocean during the last glacial. Cent. Nat. Rech. Sci. Colloq. Int. 219, 203.
Sigman, D.H., Jaccard, S.L., Haug, G.H., 2004. Polar ocean stratification in a cold climate. Nature 428, 59–63.
Steph, S., et al., 2010. Early Pliocene increase in thermohaline overturning: a precondition for the development of the modern equatorial Pacific cold tongue. Paleoceanography 25, PA2202.
Stichel, T., et al., 2012. The hafnium and neodymium isotope composition of seawater in the Atlantic sector of the Southern ocean. Earth Planet. Sci. Lett. 317–318, 282–294.
Talley, L.D., 1996. Antarctic intermediate water in the south Atlantic. In: Wefer, G., Berger, W.H., Siedler, G., Webb, D.J. (Eds.), The South Atlantic: Present and Past Circulation. Spinger, Berlin, Heidelberg, pp. 219–238.
Talley, L.D., 2013. Closure of the global overturning circulation through the Indian, Pacific and Southern Oceans: schematics and transports. Oceanography 26 (1), 80–97.
Tanaka, T., et al., 2000. JNdi-1: a neodymium isotopic reference in consistency with LaJolla neodymium. Chem. Geol. 168, 279–281.
Toggweiler, J.R., Dixon, K., Broecker, W., 1991. The Peru upwelling and the ventilation of the south Pacific thermocline. J. Geophys. Res. 96, 20467–20497.
Tsuchiya, M., 1989. Circulation of the Antarctic intermediate water in the north Atlantic Ocean. J. Mar. Res. 47, 747–755.
Wainer, I., et al., 2012. Changes in the intermediate water mass formation rates in the global ocean for the Last Glacial Maximum, mid-Holocene and pre-industrial climates. Paleoceanography 27 (3). https://doi.org/10.1029/2012PA002290.
Wilson, D.J., et al., 2013. Reactivity of neodymium carriers in deep sea sediments: implications for boundary exchange and paleoceanography. Geochem. Cosmochim. Acta 109, 197–221. https://doi.org/10.1016/j.gca.2013.01.042W.
Winckler, G., et al., 2016. Ocean dynamics, not dust, have controlled equatorial Pacific productivity over the past 500,000 years. Proc. Natl. Acad. Sci. https://doi.org/10.1073/pnas.1600616113, 201600616.
Wu, Yingzhe, 2019. Investigating the Applications of Neodymium Isotopic Compositions and Rare Earth Elements as Water Mass Tracers in the South Atlantic and North Pacific. Ph.D. thesis. Columbia University.
Zimmermann, H.B., 1983. Clay mineral stratigraphy of the Rio Grande rise and southern Brazil basin, western South Atlantic ocean. In: Barker, P.F., et al. (Eds.), Init Repts. DSDP, 72. U.S. Govt. Printing Office, Washington, pp. 383–389. https://doi.org/10.2973/dsdp.proc.72.108.1983.